A&A 512, A38 (2010)
DOI: 10.1051/0004-6361/200913071

Astronomy & Astrophysics

Using the Sun to estimate Earth-like planets detection capabilities

I. Impact of cold spots

A.-M. Lagrange, M. Desort, and N. Meunier

Laboratoire d'Astrophysique de l'Observatoire de Grenoble, Université Joseph Fourier, BP 53, 38041 Grenoble, France
e-mail: Lagrange@obs.ujf-grenoble.fr

Received 5 August 2009 / Accepted 28 October 2009

ABSTRACT

Aims. It is known that stellar spots may in some cases produce radial velocity (RV) signatures similar to those of exoplanets. To date, the most extensive set of data on spots, active regions, and activity in general for any star is that obtained for the Sun. To investigate the impact of these spots, we aim to study the detectability of Earth-mass planets in the habitable zone (HZ) of solar-type stars, if covered by spots similar to sunspots.

Methods. We used the sunspot properties recorded over one solar cycle between 1993 and 2003 to infer the RV curve that a solar-type star seen edge-on would exhibit, if covered by these spots. We also derive interesting parameters such as bisector velocity span (BVS) and photometric curves, commonly used in the analysis of RV data. We compare the obtained data with archival solar data available for the same epoch (e.g., irradiance, Ca index). We also simulate the RV of such a spotted star surrounded by an Earth-mass planet located in the HZ.

Results. The RV of the spotted star appears to be very variable, in a complex way, depending on the activity level, with amplitudes from a few tens cm/s up to 5 m/s (assuming $\Delta T_s = T_\odot - T_{spot} = 550$ K). A correlation between the BVS and the RV data is observed even when several spots are present with a slope so small that only data of very high precision (better than 5 cm/s) can enable its detection. Photometric variations of up to 0.5% are predicted, depending on the level of activity, in agreement with measured solar photometric variations.

Based on present assumptions, the detection of a 1 M_{Earth} planet located between 0.8 and 1.2 AU requires intensive monitoring (weekly or more frequent), over several years. The temporal sampling is more crucial than the data precision (assuming precisions in the range [1−10] cm/s). Cooler spots may become a problem for these detections. We also anticipate that plages, not considered in this paper, could further complicate or even compromise such detections.

Key words. planetary systems – Sun: activity – sunspots – techniques: radial velocities

1. Introduction

Most exoplanets have been detected so far around main sequence stars[1] using RV technique. Their periods range between a few days and a few (up to 5) years. Even though most of them are giant planets, a population of super Earth (lighter than 10 M_{Earth}, down to 2 M_{Earth}, Mayor et al. 2009) planets have been detected using very precise RV measurements. In the future, much effort will be devoted to the search for even lighter planets, using improved instruments and sometimes larger telescopes such as the ELTs (D'Odorico et al. 2007).

However, it has been suspected for a long time that stellar activity and pulsations could also produce RV variations that could in some cases, mimic those of RV planets. This might lead to misinterpretations of RV variations, especially when these variations have periods less or equal to the star rotational period. This actually happened in the case of TW Hydrae (Huelamo et al. 2008) or LkCa19 (Huerta et al. 2008). To investigate the impact of stellar spots, Saar & Donnahue (1997) made first estimations of the impact of a stellar spot and convective inhomogeneities on the RV curve of FeI lines. In the case of an equatorial spot of a star seen edge-on, they showed that RV amplitudes of up to 50 m/s could be produced by spots or convective inhomogeneities, depending on the spot size, the projected rotational velocity of the star and star age. The impact of spots was also investigated by Hatzes (2002) using the CaI 643.9 nm line, which lead to the conclusions that RV variations in the range of a few m/s could be observed because of spots. We note that Saar & Donnahue (1997) also pointed out that convective inhomogeneities can lead to even larger RV variations, especially for G2V type stars.

We investigated in detail the impact of stellar spots on the RV and photometric curves, and on other diagnostics commonly used to differentiate between the effescts of stellar activity and planets on RV surveys (Desort et al. 2007). We simulated the optical spectra of stars with various spectral types from F to K type, projected rotational velocities, and orientations, covered with spots of different size and latitude. From the obtained, simulated spectra, we derived the RV, photometric, and astrometric variations using the same tools as those used in the exoplanet searches, and assuming that the spectrograph used was HARPS (Mayor et al. 2003). We showed that the impact on RV studies is indeed far from being negligible and that for stars of low $v \sin(i)$, RV curve, bisector/span variations, and photometric variations may not be enough to clearly exclude spots as explanations of the observed variations. More quantitatively, spots with typical sizes of 1% can mimic both the radial velocity curves and bisector behaviour of short-period giant planets around G-K stars of $v \sin i$ lower than the spectrograph resolution. For stars with

[1] http://exoplanet.eu

intermediate $v \sin i$, smaller spots may produce similar features. These spots may therefore complicate the search for low-mass planets on orbits with periods of the order of the star rotational period. Additional observables (e.g., photometry, spectroscopic diagnostics) are in these cases mandatory for confirming the presence of short period planets, but unfortunately, photometric variations may in some cases be too small to clearly exclude spots as explanations of the observed variations. This is particularly important when searching for super-Earth planets.

Another criterion often used to distinguish spots or stellar activity in general from planets is the so-called Ca activity indicator, either expressed in terms of S index or in terms of R'_{HK}. Stars with $\log(R'_{HK})$ smaller than about −5.0, which corresponds to the value measured for the Sun at its minimum of activity (see below), are usually considered to be inactive on levels of RV variations of 2−10 m/s. Many detections of very light planets are based on this assumption.

Desort et al. (2007) study, and other studies quoted above assumed one spot at the surface of the star. The example of our Sun shows that the spot pattern is far more complex, with, often, several spots, of different size and lifetime present at a given time on the visible hemisphere. The number of spots and their size (which determine the filling factor) also strongly vary during the solar cycle. It would be interesting to know the so-called integrated Sun RV variations, analyzed in the same way as in RV searches for exoplanets. However, RVs of the integrated solar disc are intrinsically very difficult to obtain, and to our knowledge, the rare measurements available were performed using individual lines rather than using a large number of lines (which averages out individual line contributions) and the resulting RV curves differ from one author to another, with in particular amplitudes ranging from smaller than 4 m/s (McMillan et al. 1993) to 16 m/s (Jimenez et al. 1986) or greater than 25 m/s (Deming et al. 1994). Hence, quantitatively precise results about the integrated Sun RV variations are still lacking, in contrast to the precise and well documented integrated Sun brightness variations recorded over several cycles (see e.g., Fröhlich & Lean 1998; Lockwood et al. 2007; and Livingston et al. 2007).

To test the impact of spots on stellar RV variations in a more realistic way, we decided to use original sunspot data to compute the observables that would be derived when observing a solar-type star covered with spots identical to those observed on the Sun. To do so, we have used the reported sunspot patterns observed during a full solar cycle to synthetise the spectra of this "integrated" Sun and measure a number of observables (e.g., RV, BVS, and their assoicated periodograms), and estimate the associated photometric variations. Our approach is described in Sect. 2. The results are provided in Sect. 3 and compared to available data on the solar variability in Sect. 4. We then simulate the RV curve of a similarly spotted star surrounded by a 1 $M_{\rm Earth}$ planet located in the habitable zone (Sect. 5), and derive some conclusions about the detectability of these planets based on the present assumptions and in the framework of forthcoming RV instruments (Sect. 6).

2. Description of the simulations

2.1. Input solar data

To construct our spot patterns, we use the Debrecen heliographic data (Győri et al. 2003), a catalogue of positions and areas of sunspots extracted from white-light full-disk images of several observatories, including the Debrecen observatory. For this work, we used data covering more than a complete solar cycle, between Jan., 1st, 1993 and Dec., 31, 2003, representing 3700 days of observations. The temporal sampling is about 1 day. All spots with area larger than 10^{-6} of the solar hemisphere (1 micro hemisphere) were taken into account. Figure 1 shows an example of an observed map and the simulated spotted surface for JD 2 451 686. Over the whole period, more than 160 000 spots were then considered. Their position (latitude, longitude) as well as their surface assumed to be circular, were recorded and used as inputs to our simulation tool. The projected filling factor $f_{\rm p}$ (i.e., the projection of the spot surface over the Sun hemisphere) over the whole period is indicated in Fig. 2.

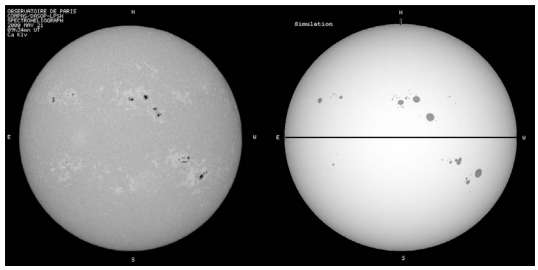

Fig. 1. *Left*: Sun surface observed with the Paris Observatory Spectroheliograph on JD 2451686. *Right*: simulated surface with spots derived from Debrecen Heliographic Data on the same day (see text).

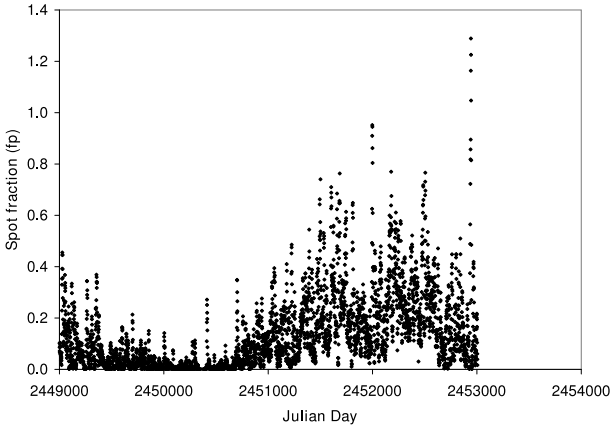

Fig. 2. Temporal variations of the projected filling factor over the whole period (see text).

2.2. Simulated spectra

For the 1993−2003 period, we used all spots larger than one micro hemisphere and produced 3700 integrated spectra, as described in Desort et al. (2007). We assume that the star is seen edge-on (indeed, it is not possible to add an inclination because we wish to rely only on observed spots). The visible, spotted, 3D hemisphere is divided into cells of size adapted to both the spectral resolution of an HARPS-like spectrograph and the minimum size of the spots considered. We then compute the resulting spectrum, assuming that each unspotted cell emits a solar-like spectrum and that each spotted cell emits like a black body of a temperature $T_{\rm s}$. The spots are then assumed to have a uniform temperature. Most of the time, we assume that $T_\Theta - T_{\rm s} = \Delta_T = 550$ K. This temperature is compatible with the bolometric spot contrast of 0.32 usually used in irradiance reconstructions (see Chapman et al. (1994), who observed contrasts ranging from 0.21 to 0.38), which corresponds to a Δ_T of about 500 K. Krivova et al. (2003) used a ΔT of 1070 K for spot umbra and 370 K for the penumbra, which is also compatible

with our value assuming a realistic umbra to penumbra ratio. The ratio of the total area of the sunspots to the umbral area varies in the literature but is typically between 4 and 6 (Solanki 2003). Assuming a typical temperature contrast of 1500 K for the umbra (a range of 1000−1900 K is given by Solanki 2003) and of 300 K for the penumbra (a range of 250−400 K is given by Solanki 2003), we infer an average temperature contrast of between 600 K and 504 K, respectively, so our adopted value is consistent with these results. However, we point out that 1) the precise temperature contrast reproducing the correct photometric contribution of the spots to the total solar irradiance depends on the actual spot data set used; and 2) the spot temperature may differ from one spot to the other (see e.g., Chapman et al. 1994). We also consider different spot temperatures, that are representative of stellar spot temperatures (Berdyugina 2005). Summing up the contribution of all cells provides the spectrum of an integrated "spotted Sun" (we refer in the following to a spotted Sun to indicate that we took into account only the spots at the Sun's surface).

Our first purpose is to identify the specific noise (jitter) induced by the spots; we therefore do not add any instrumental or photon noise to the simulated data in the first step (Sects. 3 and 4). Noise will be considered when simulating a planet signal around the spotted star (Sect. 5).

2.3. Computation of the various observables

We then used the SAFIR software (see Galland et al. 2005) to compute the RV, the CCF, and the corresponding bisector span and bisector curvature (see again Galland et al. 2005). We therefore use the same procedure as the one we use to search for exoplanets around stars with RV techniques. We also compute the associated photometric variations at 550 nm.

Since the whole process is quite time-consuming and we deal with an large number of spectra (10 to 100 times larger than the number usually used to establish exoplanet detections), we used only one order per spectrum (order 31) instead of the entire spectrum. It is acceptable to do so since considering either one order or the whole spectrum provides similar velocities (within 10%; Desort et al. 2007).

2.4. Simulation of a spotted star with planets

Finally, we compute the RV curve obtained from a star covered by these spots and surrounded by a planet in the HZ (see Sect. 5). To do so, we simply add the spot and the planet contributions. To study the planet detectability, we have to take into account a noise contribution; we therefore add random noise to the radial velocities of levels corresponding to the precisions expected for forthcoming instruments.

3. Results: spotted Sun variability over the period 1993–2003

We now first provide the results of the simulations in terms of RV, BVS, and photometric variations, assuming that the spot temperature is 550 K lower than the solar effective temperature. We then briefly study the impact of the spot temperature on these results.

To compare our results with published data on solar variability, we chose one period of reference for low activity, from 1996 July 1 (JD 2 450 266) to 1997 April 1 (JD 2 450 540), and one period of reference for high activity, from 2000 February 1 (JD 2 451 576) to 2000 November 1 (JD 2 451 850). The low and high activity periods have then durations of approximately 10 solar rotational periods. They correspond to average values of R'_{HK} of approximately −4.85 and −5.0 respectively. By assuming an average S index of 0.170, an amplitude of variations of 0.017 for the S index, as derived from Lockwood et al. (2007), a $B - V$ of 0.66, and by using the empirical relation of Noyes et al. (1984), we indeed infer R'_{HK} of between −4.88 and −4.97. These values should be regarded as indicative because the average S values depend on the dates of measurements, and to second order, on the adopted values of $B - V$, which is why the published values generally vary from one author to another.

3.1. RV variations

The resulting RVs are clearly variable over the entire cycle, as can be seen in Fig. 3. The RV curve is also far more complex than predicted by simple modeling of one spot located on a star viewed edge-on (see e.g., Saar & Donnahue 1997 or Desort et al. 2007), in which case the spot signature is present over half the stellar rotation period (when the spot is on the visible hemisphere).

The amplitude of the RV depends strongly on the filling factor of the spots, as can be seen in Fig. 4. During the low activity phase as defined above, apart from few (3) peaks at velocities larger than 40 cm/s (absolute value), the RV signal is quite "flat". The rms of the RV during this low activity period is about 16 cm/s, however it is dominated by the few peaks present during the period. During the defined high activity phase, the RV signal is far more variable and of much higher amplitude: the rms is more than 3 times higher (60 cm/s), and reaches absolute values as high as 2 m/s. We note however that the highest RV peak during the entire cycle is almost at 5 m/s. Table 1 provides the RV rms for the whole cycle and these reference periods.

Figure 3 also shows the Lomb-Scargle periodograms of the RV when considering, respectively, the whole cycle, and both the low and high activity periods. When considering the whole cycle, we observe a peak at the Sun rotation period and one at half a rotation period with a FAP ≤1%. The period at half a rotation period could be caused by "active longitudes" (spots are not distributed randomly in longitude, but it seems that two persistent "active longitudes" separated by 180° have been observed to persist over more than one century (Berdyugina & Usoskin 2003). It could also be due to the lifetimes of the large spots, which are often less than 2 solar periods (lifetimes of about 1.5 rotation period, for instance, could produce an additional peak at half a period). Those peaks are not detected in the yet noisier periodograms of the low and high activity periods. We note that the highest peak detected in the periodogram of the high activity period occurs at 20.8 days, which differs considerably from the solar rotation period. This shows that even when considering 10 solar rotation periods, the periodogram does not reveal the solar rotation period. We verified that considering a longer period (2000 days) enables the recovery of the two peaks seen in the periodogram of the whole cycle (see also Sect. 5).

3.2. Bisector variations

Spots induce variations in the line-shapes. One way of quantifying these line-shape variations is to measure in each spectrum, the bisector velocity span (hereafter BVS) of either a line, a set of lines or the CCF. Although individual lines are often considered in solar or stellar studies, exoplanet searches generally consider

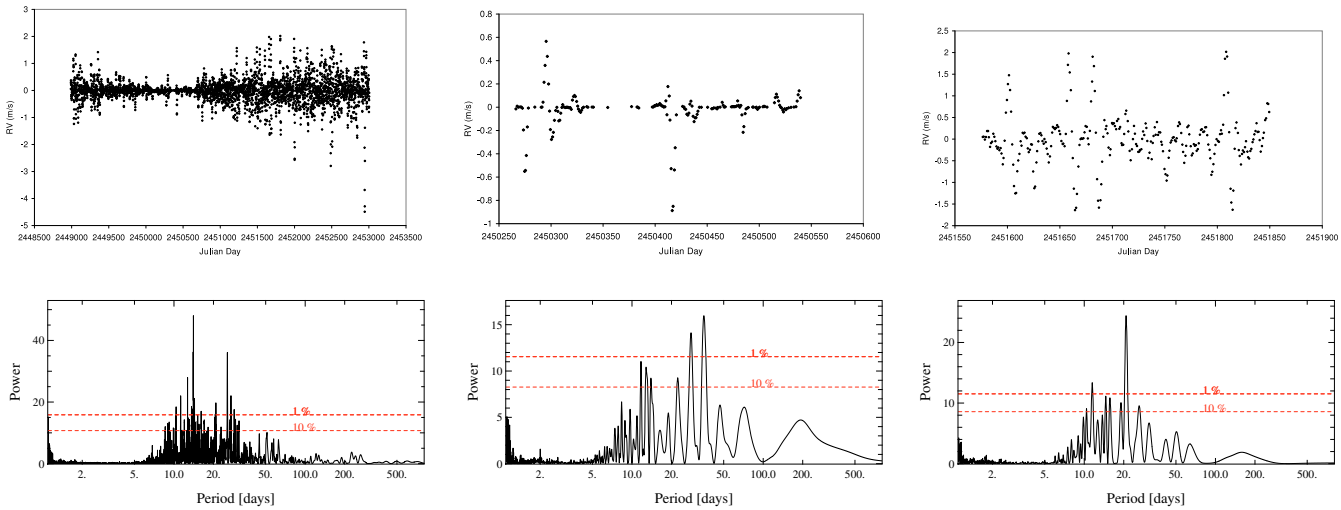

Fig. 3. Temporal variations of the RVs, and corresponding periodograms. *Left*) the whole period (JD 2 448 500 to JD 2 453 500) is considered; *middle*) the low activity period (JD 2 450 250 to JD 2 450 600) is considered and *right*) the high activity period selected (JD 2 451 550 to JD 2 451 900) is considered.

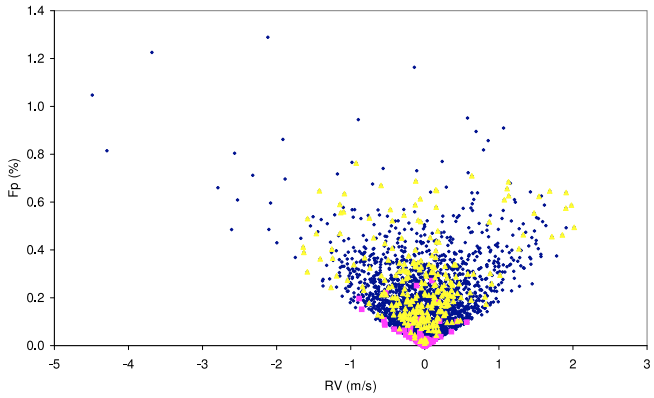

Fig. 4. RV and projected filling factor (f_p) variations over the cycle. The values corresponding to the high and low activity periods selected for reference (see text) are indicated resp. by triangles and squares. We see that the spots projected filling factors over the whole cycle vary mainly between 0 and 0.6%. The corresponding RV amplitudes vary linearly with f_p as in the case of a single spot (see Desort et al. 2008. This explains the V-shape contour of the cloud of points.

the bisector of the CCF obtained using the entire spectrum, to achieve the highest precision in determining its shape. In these studies, a correlation between RV and BVS variations is a good indicator that the RV variations are caused by spots rather than planets. However the absence of a correlation (or a flat bisector) does not necessarily mean that the RV variations are not caused by spots, as shown in Desort et al. (2007): the level of correlation depends on both the star projected rotational velocity and the spectrograph resolution.

In Fig. 5, we plot the BVS variations of our simulated spectra over the whole period. As expected, the BVSs vary with time, over the whole period. The RV and BVS variations appear moreover well correlated (see Fig. 6), as in the case of a single spot. This is true for low as well as high activity periods. The BVS/RV slope is found to be −0.037, irrespective of the activity level. The amplitude of the BVS variations is much smaller (25 times, at the level of a few cm/s) than the amplitude of the RV variations. The BVS variations will then be far more difficult to detect than the RV variations. Of course, it will be even more difficult to detect these BVS variations in noisy data; we will show below that a precision of 1 or 5 cm/s may permit the detection of the RV−BVS correlation, but a precision of 10 cm/s will not. When considering the whole cycle, the periodogram of the BVSs shows peaks at ≃14 days and at ≃7 days, i.e., at periods half of those found when considering the RV variations. A peak in the BVS periodogram at half the peak period observed in the RV periodogram can indeed be expected in the case of equatorial spots on the surface of a star seen edge-on; briefly, this is because during each quarter of a period, while the RVs maintain the same sign, the BVS sign changes (see for instance Fig. 4, bottom left in Desort et al. 2007); the number of extrema in the BVS variation curve is then twice the number of extrema in the RV variation curve. In the present case, the spots are equatorial or close to equatorial, and the Sun is seen edge-on, so the same reasonning applies. Finally, the periodograms of the BVS variations obtained when considering the low and high activity periods are, as in the case of the RVs, very noisy.

Table 1. Summary of measured rms values when modeling all sunspots.

	RV (m/s)	BSV (m/s)	Phot
$\mathrm{rms}_{\mathrm{all}}$	4.35×10^{-1}	2.0×10^{-2}	6.1×10^{-4}
$\mathrm{rms}_{\mathrm{low}}$	1.60×10^{-1}	7.9×10^{-3}	1.9×10^{-4}
$\mathrm{rms}_{\mathrm{high}}$	5.88×10^{-1}	2.6×10^{-2}	6.9×10^{-4}

Notes. RV (Col. 2); BVS (Col. 3); fr: fraction of the Sun covered by spots (Col. 3); Phot: relative photometry (Col. 4). The subscript *all* refers to the whole cycle; the subscript *low* (resp. *high*) refers to the low (resp. high) activity period.

3.3. Photometric variations

The computed photometry of our spotted Sun also shows temporal variations (see Fig. 7), of amplitude as high as 0.5% in one extreme case, but generally in the range 0−0.1%. The amplitudes of the variations strongly vary according to the cycle phase (see Table 1). Photometric variations at the 10^{-3} level, such as those predicted during the high activity period, are detectable from the ground, and actually detected when searching for transits of short period planets. They are easily detectable with spaceborne telescopes (see e.g., Mosser et al. 2009, in the

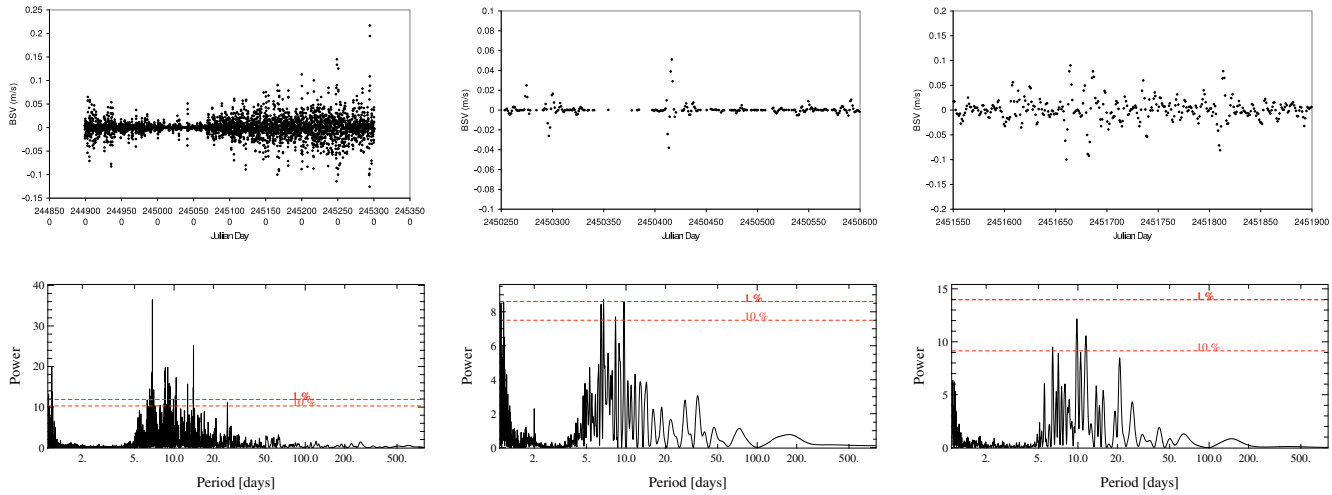

Fig. 5. Temporal variations of the BVS and corresponding periodograms, when considering the whole period (*left*), the low activity period selected (*middle*) and the high activity period selected (*right*).

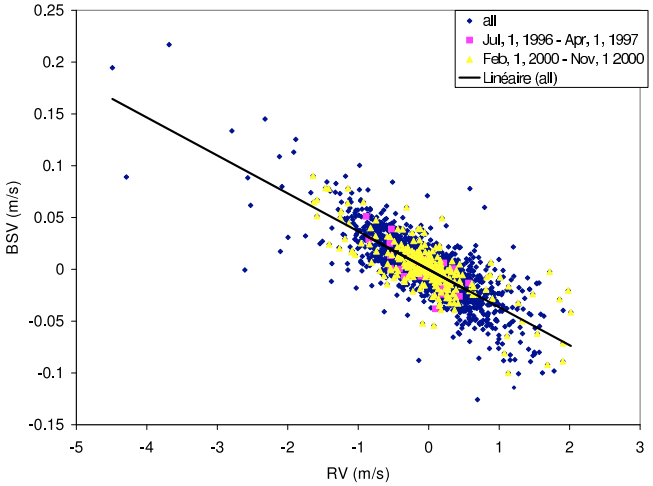

Fig. 6. Correlation between the RV and the BVS over the whole period (see text). The values corresponding to the high and low activity periods selected for reference (see text) are indicated resp. by triangles and squares.

case of Corot detection of spots around a F8 type star, associated to photometric variations of about 0.2%). The photometric variations observed during the low activity period are in contrast not detectable from the ground: the strongest peak, responsible for a RV peak at 90 cm/s on JD 2450416 produces a photometric minimum of 0.1% (on JD 2450413), and the rms of the photometric variations during the low activity period is 0.02%.

Figure 7 shows the periodograms of the photometry of our spotted Sun when considering, respectively, the whole period, and the low and high activity periods. The periodogram corresponding to the whole cycle has a peak that corresponds to the Sun rotation period, but a peak also at about 110 days. This peak is not seen in the periodogram corresponding to the low and high activity periods. We note a peak at about twice the rotation period in the case of the high activity period.

3.4. Impact of the spot temperature

In the case of a single spot, Desort et al. (2007) showed that the spot temperature has an impact on the resulting RV curve, and on both the BVS and photometric curves. We aim to briefly investigate the impact of different temperatures on the observables when considering all sunspots. This is motivated by the fact that in the case of the Sun, the temperature varies from one spot to another (e.g., Chapman et al. 1994), with a significant dependence on the spot size (e.g., Mathew et al. 2007; Wesolowski et al. 2008), and an associated dispersion of the order of a few hundreds of K. In the case of other stars, different spot temperatures are also inferred, with a possible trend between the spot temperature and the stellar effective temperature (see Berdyugina 2005 for a review).

3.4.1. Spot temperatures 1200 K lower than the Sun effective temperature

We then performed another complete simulation, as described in the previous section, assuming that the spot temperature is 1200 K (instead of 550 K) below that of the Sun. The RV variations due to spots of temperature 1200 K lower than the solar effective temperature are larger by a factor of 1.75 than those obtained assuming that ΔT_s = 550 K. They then induce a stellar jitter 1.75 times larger, which is not negligible.

Based on the same assumption, we find a BVS/RV slope of −0.037, similar to that found assuming ΔT_s = 550 K. We conclude that the BVS/RV slope is insensitive to the temperature, within the considered temperature range. The ratio BVS(1200)/BVS(550) is also found to be 1.75, i.e., similar to that obtained for the RVs. Finally, the amplitude of the photometric variations for the cooler spot is found to be larger by a factor of 1.8 than that produced by the warmer spot. We note that the amplitude of the photometric variations during the low activity period is still below the precision achievable in ground-based observations.

3.4.2. Various spot temperatures

To investigate other temperatures, we limited our simulations to the case of a single spot with various temperatures 200, 400, 600, 1000 and 1200 K lower than the Sun effective temperature. We first check that the ratio $V_{\rm Max}$ (1200)/$V_{\rm Max}$ (550), where $V_{\rm Max}$ (550) (respectively $V_{\rm Max}$ 1200) represents the maximum RV amplitude assuming ΔT_s = 550 K (resp. 1200 K), is consistent with the ratio obtained when considering the entire set of spots. The maximum RV obtained in each case is plotted as a

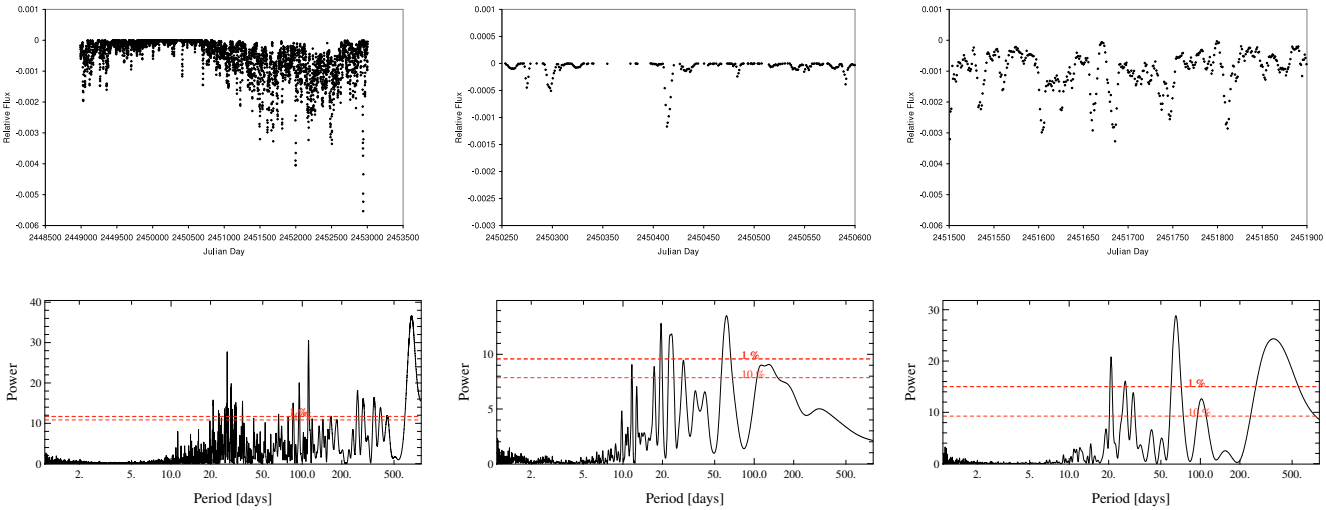

Fig. 7. Temporal variations of the spotted Sun relative photometry (ie compared to a Sun without any spot) and corresponding periodograms, when considering the whole period (*left*), the low activity period selected (*middle*) and the high activity period selected (*right*).

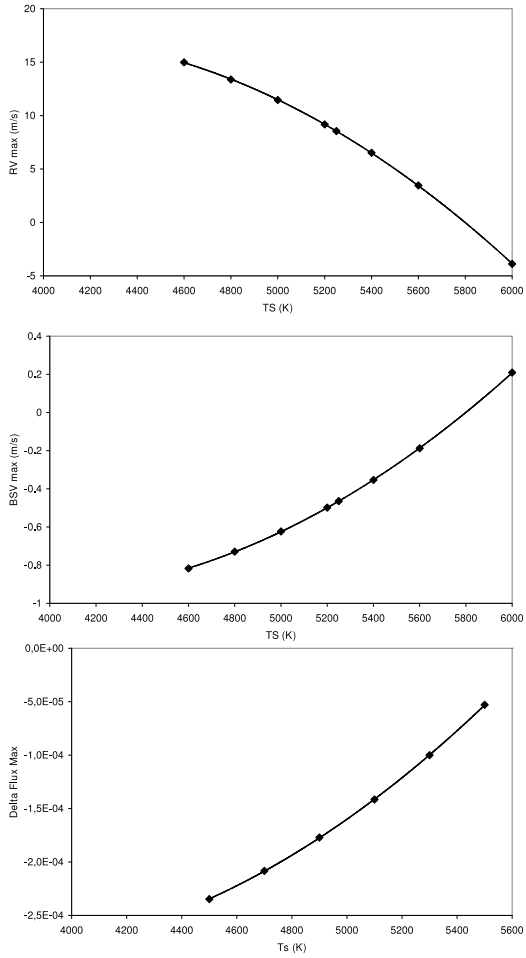

Fig. 8. Maximum RV (*top*), BVS (*middle*) and spot absorption (*bottom*) assuming different spot temperatures.

function of the spot temperature in Fig. 8. Figure 8 also gives the maximum BVS and the maximum flux absorption as a function of the spot temperature. We see that the spot temperature has a significant effect on these observables, with larger amplitude signals in the case of cooler spots. These figures allow us to estimate the RV, BVS, and photometric variations for any spot temperature.

4. Comparison with published data for the integrated Sun over the period 1993–2003

4.1. Radial velocity data

The amplitude of our computed RV variations has an rms of 60 cm/s and may be as high as 5−6 m/s during the high activity period. As already mentioned a few peaks at 1 m/s may be found during low activity periods, but the rms of the variations is much smaller during the low activity period.

Jimenez et al. (1986) published actual RV measurements for the integrated Sun between 1976 and 1985 (cycle 21), collected with a resonant scattering spectrometer. The strongest variations are obtained in 1982, which amplitudes are of about 16 m/s at maximum activity.

McMillan et al. (1993) published RV measurements obtained for the period 1987−1992, measured on spectra of the sunlit surface of the Moon, in the blue part of the spectrum, between 425 and 475 nm. They did not detect variations larger than 4 m/s over this 5 year period. However, they noted that the lines present in the considered spectral range could be less sensitive to activity than other lines, such as those considered by Jimenez et al. (1986). During the same period, between 1984 and 1992, Deming et al. (1994) also recorded RV variations of the integrated Sun, using the CO lines at 2.3 microns. Their measurements revealed variations with peak-to-peak values of about 25 m/s.

Our simulated RV amplitudes are smaller than those measured either by Jimenez et al. (1986) or Deming et al. (1994). This might be because the Sun was less active in cycle 23 than in previous cycles. It might also be because we take into account only spots and not plages and convection in the present simulations (but see below), or because our predicted RVs are "measured" on the CCF and not on single lines. However, the strong discrepancies between the published measurements prevent us from deriving firm conclusions, and from validating or not our simulations.

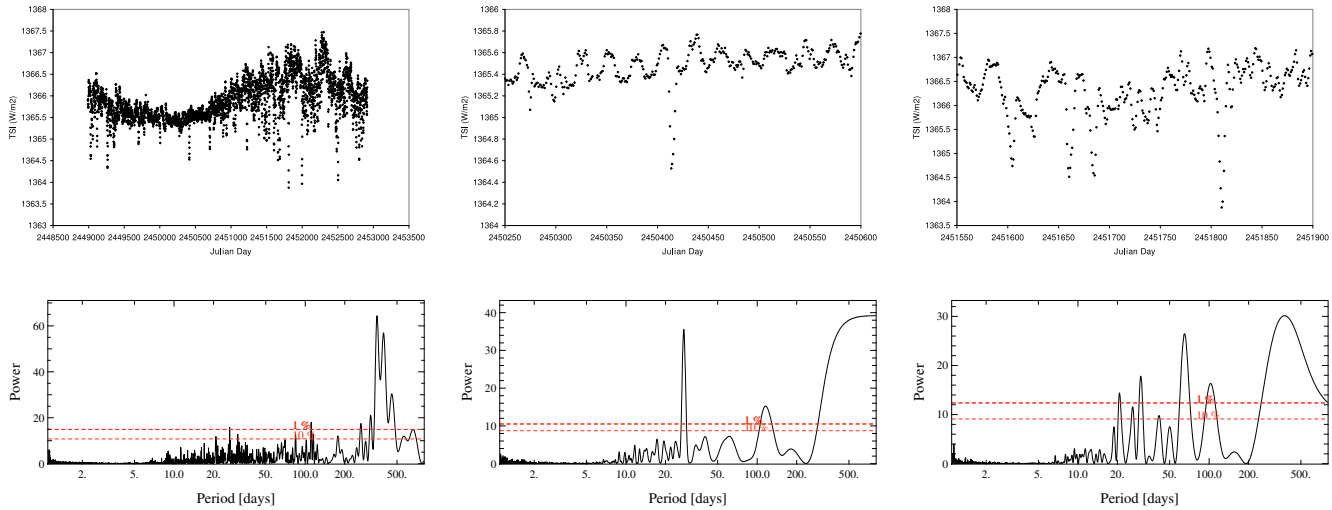

Fig. 9. TSI temporal variations, and corresponding periodograms when considering the whole period (*left*), the low activity period selected (*middle*), and the high activity period selected (*right*).

4.2. Photometric data

We compare our simulated photometric variations caused by spots with the measured photometric data such as the total solar irradiance (hereafter TSI), the measured spectral solar irradiance (hereafter SSI). We attempt to test our spot model, even though we do not expect this model to fully reproduce the Sun photometric variations because it is well known that plages strongly contribute to the Sun's brightness variations (see below).

4.2.1. Total solar irradiance (TSI)

We first compare our computed photometric variations caused by spots to the observed total solar irradiance (TSI) variations during the period 1993−2003, compiled by Claus Fröhlich and Judith Lean[2]. Figure 9 provides the measurements recorded over the whole cycle, as well as zoomed variations during our two reference activity periods. It also shows the corresponding periodograms.

Over its cycle, the Sun's observed brightness (see e.g., Fröhlich & Lean 1998; and Lanza et al. 2007a,b) increases with the activity produced by the plages. In addition, sharp brightness decreases are sometimes observed, due to spots. A relative difference of about 1 W/m^2 is observed in the TSI between the solar minimum average and the maximum average. From Fröhlich & Lean 1998 reconstruction of the plages and spots contributions, it seems that plages dominate the long timescale variations, producing photometric amplitudes of about 2 W/m^2 during this cycle and that the spots contribution to the long-term variations is twice as small (relative intensity of about 0.9993). In addition, the spot contribution to the short timescale variations may be significant, the transient absorption peaking at up to 3−4 W/m^2. These values for the peaks due to spots are in excellent agreement with our simulated photometric variations as can be seen when comparing Figs. 7 and 9, especially during the low and high activity periods. For instance, the isolated simulated narrow peak (during low activity), due to a spot, is observed simultaneously in the TSI curve and the simulated intensity on JD 2450413 with respective intensities of ≃0.07% and ≃0.11%. The discrepancy between the simulated photometric variations (0.11%) and the TSI curve variations (0.07%) is rather small, given that the TSI variations are not caused entirely by spots, but also by plages. We therefore do not try to attribute it to physical effects (such as a lower spot temperature in our simulated spots). The temporal variations of the TSI and simulated photometry are also remarkably similar during the high activity period, even when several spots are present on the visible hemisphere at a given time. We then conclude that the present simulations of sunspots are accurate and that the assumption of a single temperature for the sunspots is acceptable. Therefore, we can apply the simulation results safely to solar-type stars for which the activity is dominated by spots.

The comparison between simulated and observed data also confirms that the short timescale photometric variations of the Sun during high activity are quite sensitive to the spots, and that the variations in the Sun brightness during the low activity period are not dominated by the spots. Consequently, we can stipulate that, as far as the Sun is concerned, our simulations provide a good enough description of its RV variations during the high activity period but may not provide a good estimation of the Sun RV variations during the low activity period.

The good agreement between the TSI variations and the simulated photometric variations during the high activity period can also be seen in Fig. 10, where we have plotted the TSI and simulated spot flux absorptions when considering the days (3568 days over the cycle) for which we have both spot identifications (hence photometric data from our spot simulations) and actual TSI measurements. Although we do not see any overall correlation between both quantities if we consider the whole cycle (or the low activity period, except in the rare cases when spots are present), we see a rather good correlation when we focus on the high activity period.

The periodogram of the TSI (Fig. 9) over the whole cycle is quite noisy; it has one peak at the Sun rotation period, which is also seen in the simulated data (Fig. 7), with an associated false alarm probability lower than but close to 1%. It also contains other peaks, of however lower associated confidence level, in particular at about 20 days; the discussion of these peaks is beyond the scope of the present paper, and we refer to Hempelmann et al. (2003) for addtional discussion. The periodogram corresponding to the low activity period appears to be quite different. In particular, the very clear (with FAP much lower than 1%) peak observed at 26 days in the TSI

[2] http://www.ngdc.noaa.gov/stp/SOLAR/

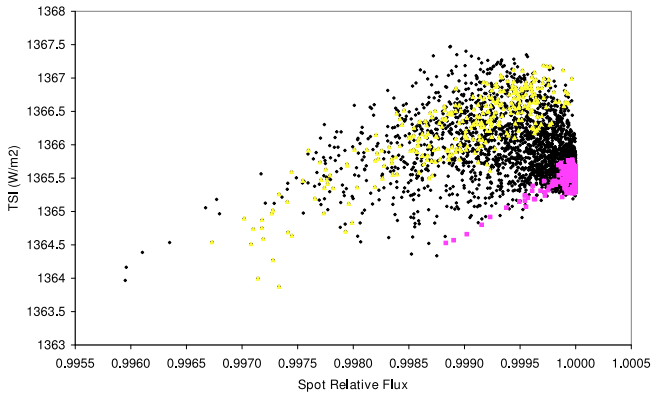

Fig. 10. TSI and spotted Sun photometry over the whole period. The values corresponding to the high and low activity periods selected for reference (see text) are indicated resp. by triangles and squares.

periodograms is not seen in the periodogram of the corresponding simulated data, which is quite coherent with what is directly seen in the photometric curves (strongly modulated signal). In contrast, the periodogram corresponding to the high activity period appears to be more similar to the simulated one; in particular, they both have a peak at about twice the solar rotation period. The similarity between both periodograms is again in agreement with the short timescale variations being more sensitive to the spots during the high activity period.

4.2.2. Spectral solar irradiance (SSI)

Similar conclusions are reached when we compare the simulated data (Fig. 7) with the SSI data at 402, 500, and 862 nm during the reference activity periods (Fig. 6 of Lanza et al. 2004; see also Fligge et al. 1998; Fligge et al. 2000). We also note that the simulated data are in closer agreement with the 402 nm SSI data than with the longer wavelength data. This shows that the short wavelengths may be more sensitive to the spots than the longer wavelengths. In the SSI data, the spot signal has a larger amplitude in the blue part of the spectrum than in the red. We note that this is also true for the plage signal, therefore it is clear that the data at shorter wavelengths are a better indicator of activity than those at longer wavelengths.

4.3. Ca index

While the TSI variations are caused by both plages and spots (although dominated by plages on long timescales), Ca variations are due to the chromospheric emission of plages. Lockwood et al. (2007) reported on the Ca variations (S index and Ca core emission) over 3 cycles, from 1975 to 2004. As expected, the Ca variations over the 3 cycles roughly follow the solar cycles, as seen by comparing the TSI temporal variations with the Ca temporal variations (see also Livingston et al. 2007). We note that the amplitudes of both the TSI and the Ca variations vary significantly depending on the cycles; in particular, the last one (cycle 23) corresponding to the data used in the present paper exhibit the smallest amplitude among the 3 cycles, indicative of an activity level lower than during previous cycles. Importantly in the present context, we note the presence of high frequency variations in the measured Ca indices throughout cycle 23 (see Fig. 11), at maximum activity (with peak-to-peak variations greater than 0.01), but also at minimum activity (peak-to-peak variations of 0.005).

The periodogram of the Ca index for the entire cycle does not contain any significant peak apart from at 7 days and 3.5 days, which we checked are also present in the periodogram of the temporal sampling of the data. Some peaks may be present at about 26 days, but the associated false alarm probability is in the range 1−10%. The periodogram corresponding to the low activity period has a peak at the Sun rotation period with, however, a 10% false alarm probability. Finally, the periodogram of the high activity period does not provide valuable information. This shows that the Ca index periodogram hardly provides any valuable quantitative information about the periodicities involved, even though we study with a relatively large amount of data.

Since the Ca index variations are mostly controlled by the plages, we do not expect to find a clear correlation between the Ca index and the presence of spots. This is confirmed in Fig. 12, where we show the (RV−Ca index) diagram corresponding to the days (1134 in total) in period 1993−2003, for which the spot simulations and the Sacramento Peak Solar Observatory Ca index measurements from the database[3] are available at the same time. However, we see that the higher RV amplitudes are found during periods of high Ca indices. This is consistent with the largest spots being present during high activity periods.

4.4. Notes on the plages

Plages are large structures slightly hotter than the Sun surface. The long timescale variations in the Sun photometry are dominated by plages, even though spots do have clear signatures in terms of short timescale variations.

Spots have been inferred since several decades on the surface of stars, either dwarfs or young stars, thanks to rotation-modulated flux decreases in the photometric curve. Doppler imaging has also enabled maps of spots to be produced in the case of high projected equatorial velocities stars (early-type stars or active stars; see e.g., Donati & Collier-Cameron 1997; Skelly et al. 2008). Plages have been recently inferred from long-term (years or decades) photometric surveys (Lockwood et al. 2007) and from line profile studies of young spotted stars (Skelly et al. 2008, 2009a,b). According to Lockwood et al. (2007), the long-term photometric variability of stars with $\langle \log(R'_{\rm HK}) \rangle$ lower than $\simeq -4.75$, is plage-dominated, with an increase in brightness at maxmimum activity, as in the case of the Sun, whereas stars of $\langle \log(R'_{\rm HK}) \rangle$ greater than $\simeq -4.75$ are spot-dominated. We note however that 1) this limit value of $R'_{\rm HK}$ is approximate; and 2) Hall et al. (2009) have questioned the correlation between activity and brightness in the case of very low activity stars, as well as the pertinence of $R'_{\rm HK}$ (or the S index) for stars of low activity.

In any case, if present on the surface of stars in addition to spots, plages could a priori induce RV variations as spots do. Since our paper is devoted to the impact of spots on the RV variations, a detailed study including the plages is not presented here. However, it is interesting to roughly estimate their contribution.

To do so, we computed the contribution of a plage to the RV variations. Following Lanza et al. (2007a,b), we assumed that the temperature difference between the plage and the solar surface varies as 1-μ, where $\mu = \cos(\theta)$ and θ is the angle between the normal to the surface and the line of sight; using the plage contrasts observed by Ermolli et al. (2007), the plage temperature is then $T_{\rm p} = 5800 + 85$ (1-μ) K. We furthermore assumed a filling factor $f_{\rm p} = 20\%$ for the plage, and $f_{\rm p} = 2\%$ for the spot. Figure 13 illustrates the RV variations induced by this

[3] http://www.ngdc.noaa.gov/stp/SOLAR/

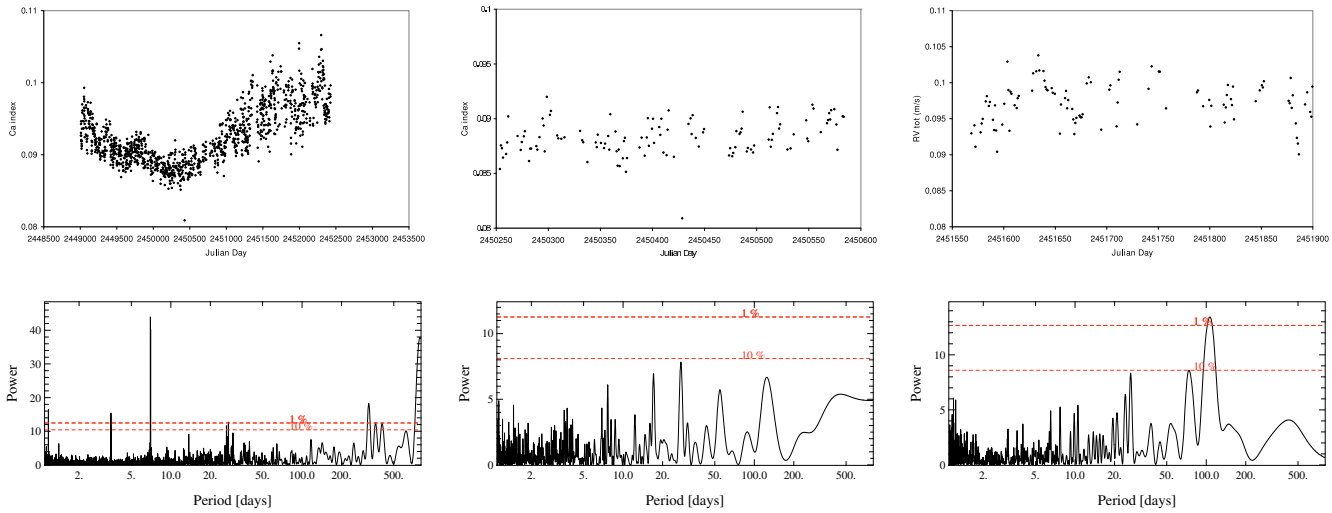

Fig. 11. Temporal variations of the Ca index, and corresponding periodograms when considering the whole period (*left*), the low activity period selected (*middle*), and the high activity period selected (*right*).

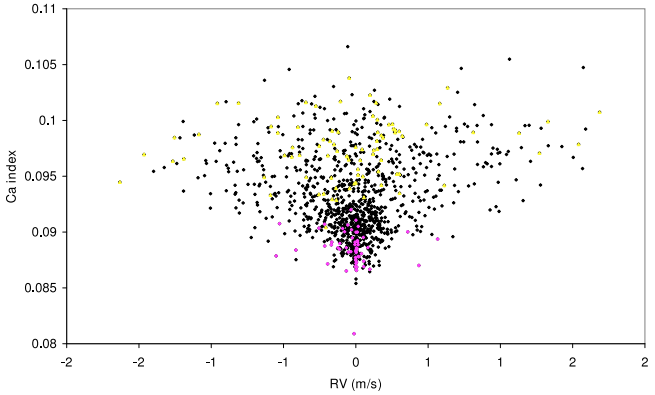

Fig. 12. Simulated RV and measured Ca index over the whole period. The values corresponding to the high and low activity periods selected for reference (see text) are indicated resp. by triangles and squares.

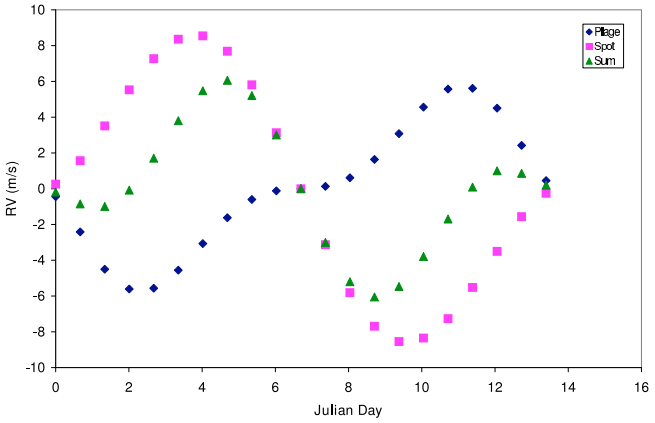

Fig. 13. Contributions to the RV variations of a spot (squares) and a plage (diamonds) with respective f_p = 2 percent and f_p = 20 percent and temperatures respectively 550 K lower and 10 K higher than the Sun surface. The total RV variations are represented by triangles.

plage located at the equator, as well as those produced by a spot 550 K cooler than the Sun. The total RV variations, produced by both the spot and the plage are also provided.

In this simple example, the RV signal due to the plage appears to be slightly lower in amplitude and of opposite sign to the RV signal produced by spots. When adding both signals, assuming implicitely that the spot and plage are seen at the same time and are centered on the same place, the effect of the plages is therefore to slightly reduce the amplitude of the RV variations due to spots alone and slightly modify the position of the RV extrema.

Of course, this is a very simplified case and the true situation is more complex, since the ratio of the plage filling factor and the spot filling factor exhibits in practice a large dispersion (Chapman et al. 2001) and many plages are seen that are not associated with spots (this is clearly seen for instance in Fig. 9 during the low activity period). The true total RV variations when considering spots and plages will therefore be more complex. We can anticipate that the low activity period will be particularly affected. If we assume that the relative impact of the spots compared to plages on the RV will be comparable to that observed on the TSI curve during the low activity period, then the plages would induce a pattern of variations with amplitudes of about 20 cm/s, strongly modulated by the Sun rotation period. As already mentioned, we expect the high activity period to be comparatively less affected by the plages, even if they are of course present.

We will develop a complete and consistent set of simulations taking into account the plages in a subsequent paper (Meunier et al. 2010). The possible impact of convective downflows, not considered here within the plages will also be investigated in this paper.

5. Earth-mass planets in the HZ of a spotted solar-type star

We illustrate here the impact of spots on the detectability of Earth-mass planets in the HZ of solar stars observed with the future generations of high precision spectrographs, such as Espresso on the VLT or Codex on the E-ELT (D'Odorico et al. 2007). We then assume that the spotted solar-type star is surrounded by a 1 $M_{\rm Earth}$ planet on a circular orbit, located at a distance of 1.2, 1 or 0.8 AU. These values are representative of the inner and outer boundaries of the HZ for a $\simeq$1 solar mass MS star (see e.g. Jones et al. 2006). For instance, in the case of the Sun, Kasting et al. (1993) find HZ boundaries of 0.95 and 1.37 AU, but the limits of the continuously habitable zone (CHZ), which takes into account the variations in the solar

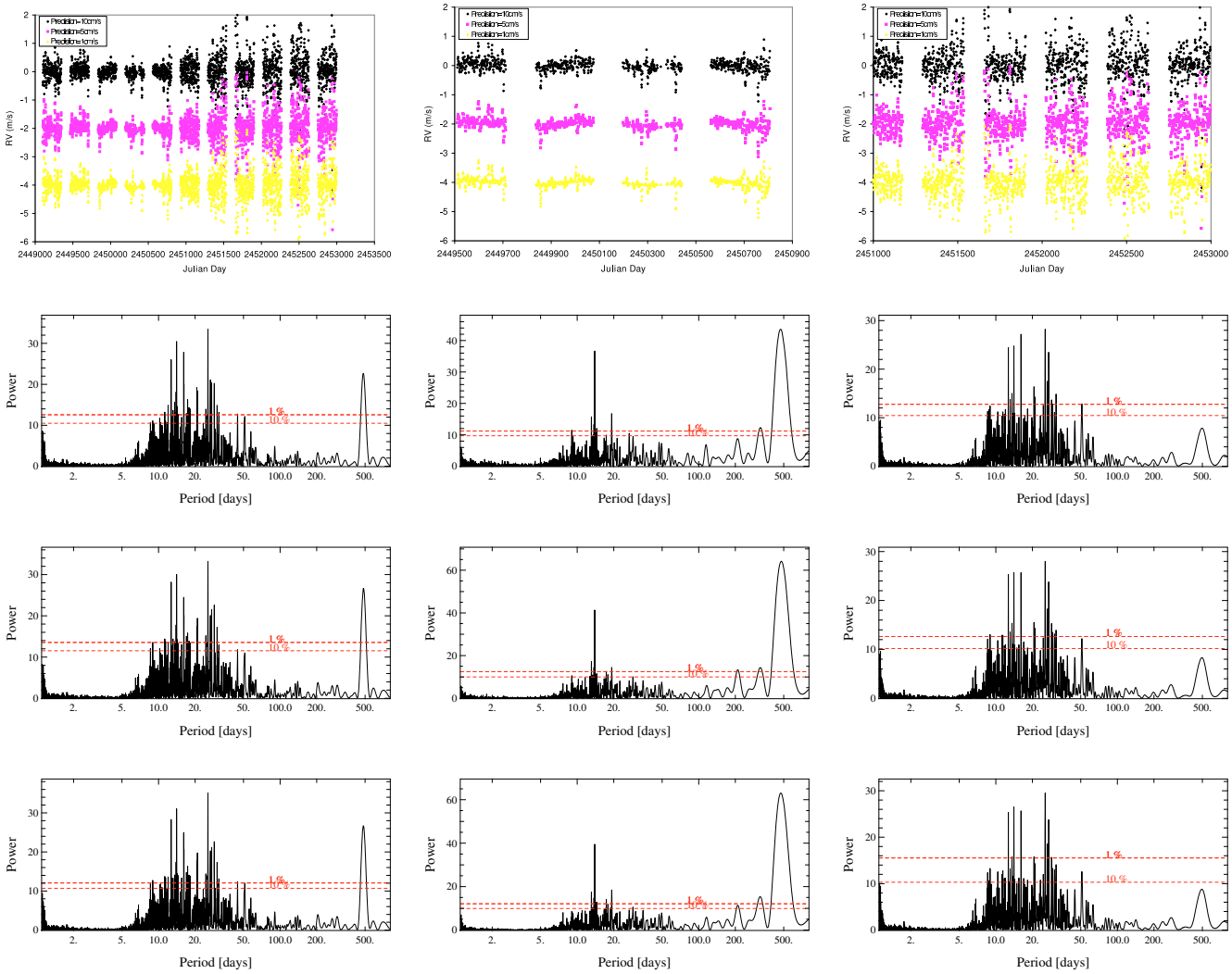

Fig. 14. *Top*: RV of a spotted solar-type star surrounded by a 1 $M_{\rm Earth}$ planet orbiting at 1.2 AU. The star is assumed to be observable 8 months per year. The RV curves correspond, *from top to bottom*, to precisions of 10 cm/s, 5 cm/s and 1 cm/s (note that the curves for the precisions of 5 and 1 cm/s have been vertically shifted for clarity purposes). The full cycle (*left*) as well as a low activity (*middle*) and high activity (*right*) periods are considered. The corresponding periodograms are provided: first line: 10 cm/s; second line: 5 cm/s and third line 1 cm/s.

luminosity with age, are more restrictive: between 0.95 and 1.15 AU. The RV amplitudes associated with these radii are 8.1, 8.9, and 9.5 ± 0.05 cm/s, respectively, and the periods associated with these radii are about 480, 365, and 261 days, respectively. We assume that the precision of the RV data is either 10 cm/s, which corresponds to the precision requirement of the Codex instrument on the ELT, and either 5 cm/s or even 1 cm/s, which corresponds to the goal performances on the Espresso instrument on the VLT. Otherwise mentionned, we assume that the spot temperature is 550 K below the Sun effective temperature. We assume that the star coordinates are (RA, Dec) = (00:00:00, −45:00:00) and we consider that it is observable in acceptable conditions whenever its airmass is lower than 1.5, hence, given its declination, during 8 months. We then assume that the star is observed either every night during these 8 months (best temporal sampling), or every 20 nights, 8 nights, or 4 nights. We computed all RV curves and their associated periodograms for these cases (orbital radius a, temporal sampling, precisions), and attempted to fit the RV curves in a number of interesting cases. We now describe the results obtained in the case of a planet located at a = 1.2 AU, and discuss the impact of both the planet orbital radius and the spot temperature.

5.1. Case a = 1.2 AU

Figure 14 provides the resulting RVs for a one-day interval of observation, as described above, and for precisions of 10 cm/s, 5 cm/s, and 1 cm/s. The associated periodograms are also provided. These results are given for the whole cycle, as well as for low and high activity periods. We note that in this section, we extend the duration of the low and long activity periods as much as possible so as to cover several planet orbital periods: the low activity period now extends from JD 2 449 500 to JD 2 450 900 and the high activity period from JD 2 451 000 and JD 2 453 000. These periods have then durations of 1400, and 2000 days, respectively.

During the lowest activity period, we see in Fig. 14 that the planet signal is clearly visible in the RV curve at most for about 3−4 years. It is much less visible, however, in the data corresponding to the high activity period. The periodogram corresponding to the low activity period clearly reveals the planet orbital period in addition to the activity-related peak at about 14 days (which we note, was not detected when considering a 400-day period, but is well detected when this 1400-day period is considered). The FAP of the planet peak is smaller

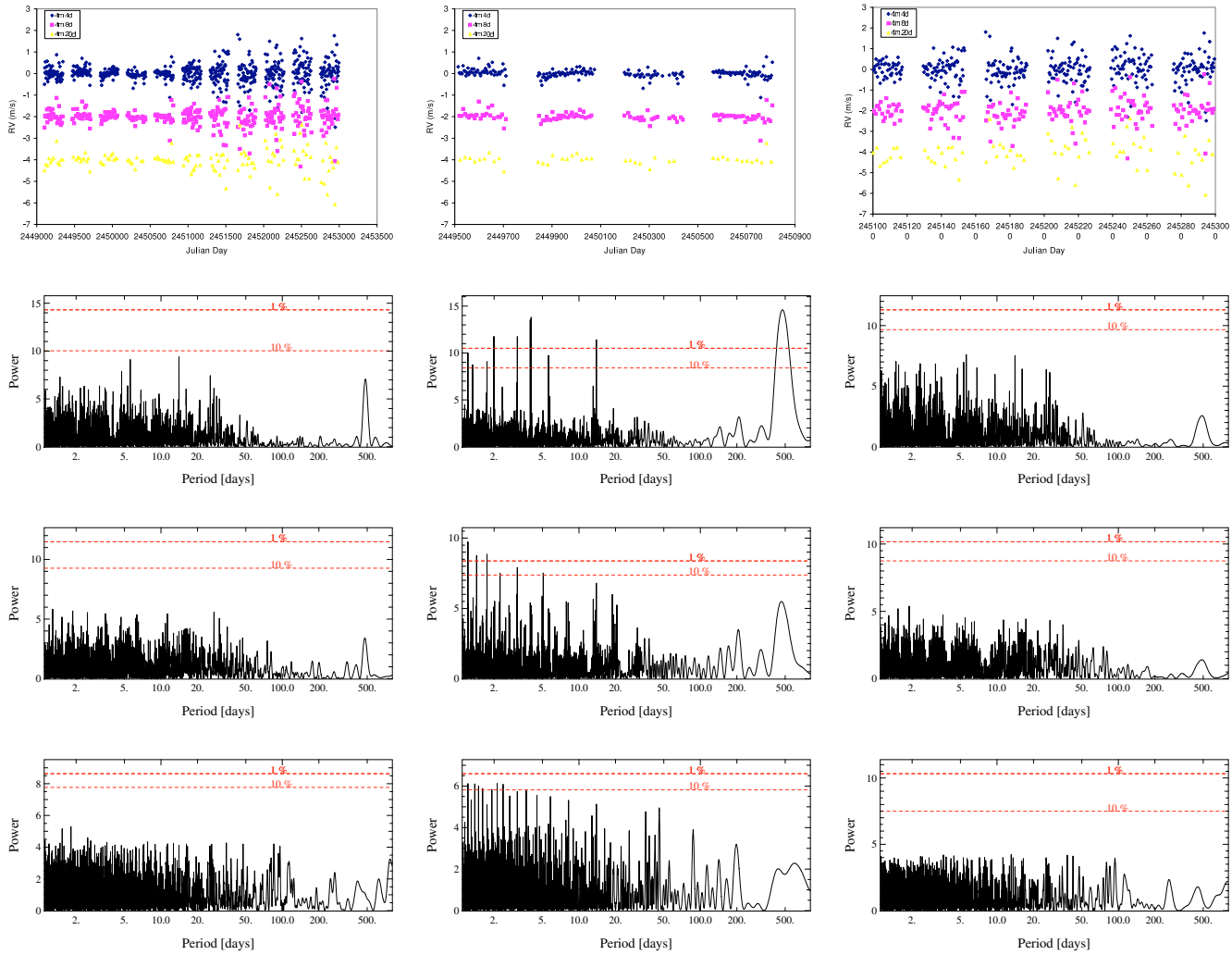

Fig. 15. Impact of the data sampling: *Top*: RV of a spotted solar-type star surrounded by a 1 $M_{\rm Earth}$ planet orbiting at 1.2 AU. The star is assumed to be observable 8 months per year and observed every 4 days (top data); 8 days (*middle data*) or 20 days (*lower data*). In all casses, we assume a precision of 5 cm/s. The RV curves have been vertically shifted for clarity purposes). The full cycle (*left*) as well as a low activity (*middle*) and high activity (*right*) periods are considered. The corresponding periodograms are provided: first line: temporal sampling is 4 days; second line: 8 days and third line 20 days.

than 1%. We note that this peak is higher than the activity-induced ones, whatever the precision assumed. When considering the whole cycle, the planet-induced peak intensity becomes fainter than the activity-related peaks, but still has a FAP smaller than 1%. When considering the high activity period, the peak associated with the planet has a FAP larger than 10%. (We note nonetheless that as it is well detached from the other peaks, it can still be identified). This is agrees with the low activity period not being strongly affected by the spots, in contrast to the high activity period. Importantly, we see that the peak detectability very marginally depends on the precision of the data in the present case.

In the case where the star is observed every 4 days (see for instance Fig. 15 for a 5 cm/s temporal sampling), the conclusions remain qualitatively similar; however, the planet peak in the periodogram is lower than in the previous case (daily observations), and only in the case of the low activity period is its FAP smaller than 1%. We note that we detect several additional peaks that are also present in the periodograms of the observing dates, and are signatures of the true data sampling. Again, the precision does not have a significant impact on our results.

When the temporal sampling is poorer (Fig. 15), the peak corresponding to the planet period becomes much less clear in the case of a temporal sampling of 8 days, with a FAP larger than 10%, and is no longer detectable in the case of a temporal sampling of 20 days during the low activity period. During the high activity period, it cannot be identified already for an 8-day sampling. Again, the precision of the data does not significantly impact our conclusions.

The precision has nevertheless a major impact on the capability of detecting the signature of the spots, as seen in Fig. 16 where we plot the (RV; BVS) diagrams assuming precisions of 1 cm/s, 5 cm/s, and 10 cm/s, as well as an infinite precision in the planet+spots case and in the spots-only case for comparison. When considering the planet+spots case, the RV−BVS correlation is quite clear when assuming no noise, or even a 1 cm/s noise. The correlation is not so clear when assuming a 5 cm/s noise and is not clear at all with a 10 cm/s noise. In the spots-only case, the conclusions are similar, as the (RV; BSV) curves are quite similar. This is because the planet induces variations with RV amplitudes smaller than 8.1 cm/s, which vary with a significantly larger amplitude due to the spots (see Sect. 3), and

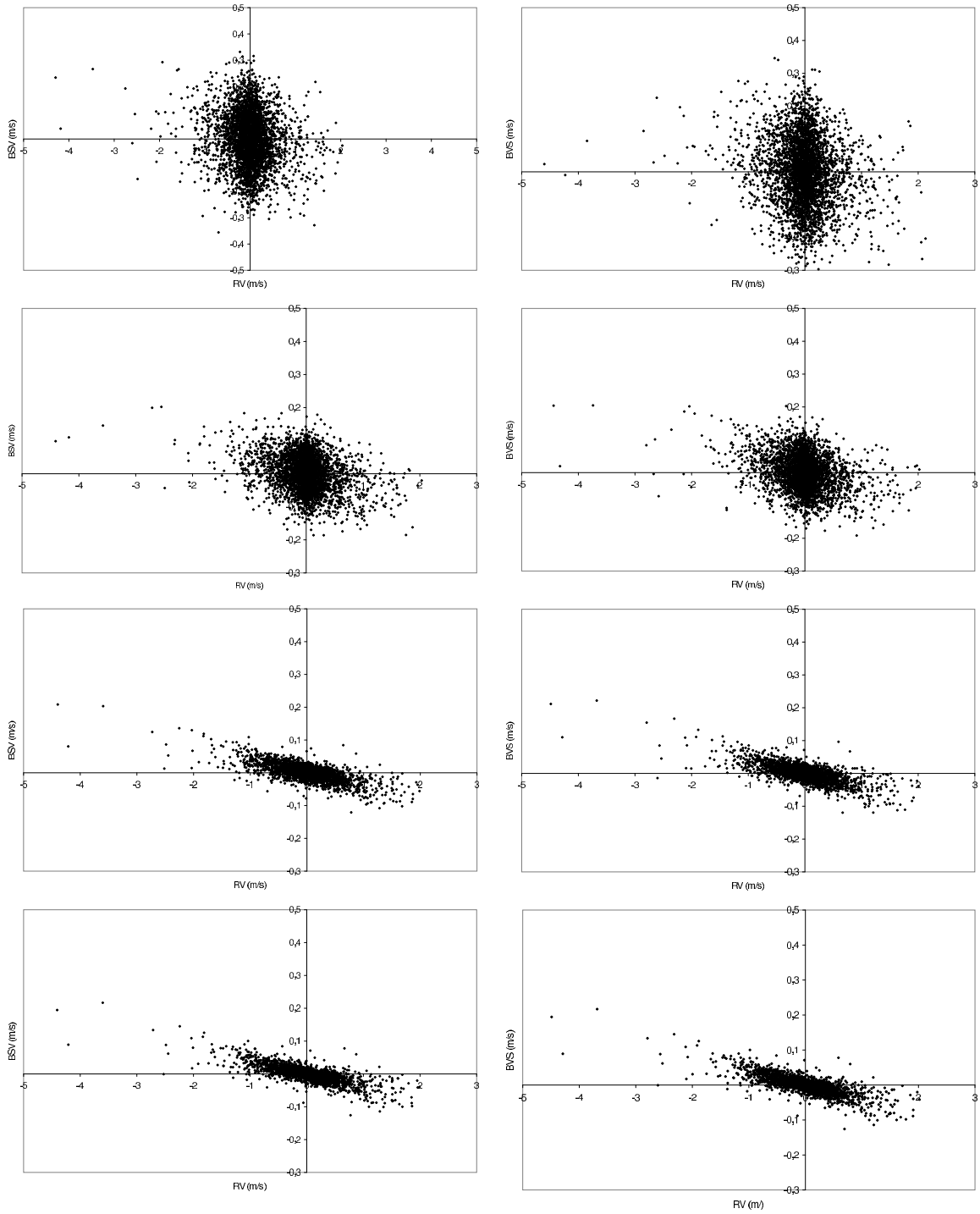

Fig. 16. *Left*: (RV; BVS) diagrams for a spotted solar-type star surrounded by a 1 $M_{\rm Earth}$ planet on a circular orbit at 1.2 AU. The star is assumed to be observable 8 months per year. *From top to bottom*, we consider precisions of 1 cm/s, 5 cm/s and 10 cm/s, as well as an infinite precision. The spot induced RV−BVS correlation is quite clear in the data without noise, and with a 1 cm/s precision; it is marginally seen when considering a precision of 5 cm/s and is lost when considering a 10 cm/s precision. *Right*: same, assuming that the spotted star is not surrounded by a planet. The correlation is quite clear in the data without noise, or with a low noise (1 cm/s), and is not so clear when considering a noise of 5 cm/s and lost when considering a 10 cm/s noise. The comparison of the left and right figures shows that in this case the planet does not impact the RV−BSV correlation.

of course, the planet does not induce BVS variations. The impact of the planet is therefore quite negligible. For a much closer or more massive planet, the conclusions would naturally be quite different.

We then tried to fit the RV curves to check whether the planet parameters (e.g., orbital radius, mass) could be retrieved. We first assumed that the star is observed with the best temporal sampling. In this case, the fit of the RV data corresponding to the whole cycle provides a minimum χ^2 corresponding to parameters close to the input values, within the uncertainties. This means that the data would permit detection of the planet and the derivation of its orbital parameters. This is also true when

considering the RV data corresponding to the low activity period. During the high activity period however, the minimum χ^2 found corresponds to small periods, typically in the range [0−30] days (corresponding to the largest peaks in the periodograms). We can still find a reasonably good fit to the RV curve providing that a range of periods, including the planet period, roughly estimated from the periodogram, is given. Similar conclusions are reached when considering data obtained with a 4 or 8 day temporal sampling. We show an example in Fig. 17 in the case of a 4-day temporal sampling and a noise of 1 cm/s. We performed 10^6 realizations of a planet RV signal with 3 parameters: the period was taken randomly to be between 0 and 1000 days, the phase between 0 and 2π, and the amplitude between 0 and the maximum of the observed signal. For each realization, the χ^2 was computed. The upper panels of the figure show the smallest values of the χ^2. In this example, we obtain at a 1σ level: $a = 1.175^{+0.022}_{-0.020}$ AU and $M = 1.21^{+0.16}_{-0.15}$ $M_{\rm Earth}$, and at a 2σ level: $a = 1.175^{+0.034}_{-0.032}$ AU and $M = 1.21^{+0.25}_{-0.25}$ $M_{\rm Earth}$. If the temporal sampling is worse (every 20 days), no good fit of the RV curve can be obtained, even when considering the entire cycle or only the low activity period.

We conclude that based on the simple assumption of a planet on a circular orbit, the planet signal can be detected, provided that the star is observed with a very good temporal sampling (superior to every 8 days), and at least over 4 periods, for the low activity period. During the high activity period ($\log(R'_{\rm HK}) \simeq -4.85$), only a very high temporal sampling would permit the detection of the planet signal, but deriving its orbital parameter becomes very difficult. The temporal sampling is crucial to detect the planet signal, whereas the precision is not so important. The interest in the RV precision remains in identifying stellar activity.

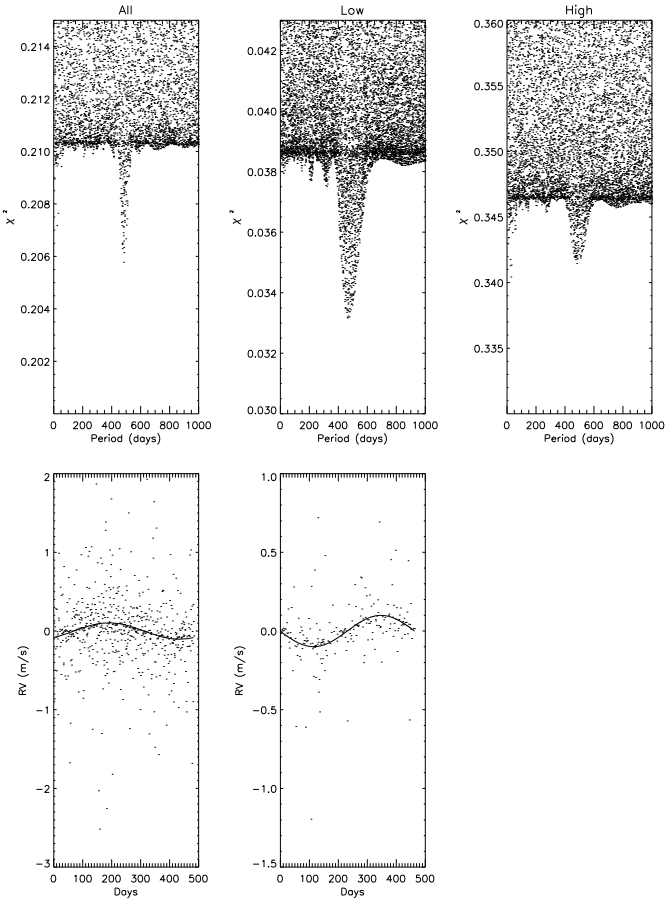

Fig. 17. Fit of the RV data and parameters found in the case of a 1 $M_{\rm Earth}$ planet orbiting at 1.2 AU. The spotted star is assumed to be observed 8 months per year, with a 4 days temporal sampling (see the corresponding RV curves in Fig. 3). A 1 cm/s noise level is considered. *Left*) the whole cycle is considered; *middle*) the low activity period is considered, and *right*) the high activity periods is considered. *Top*: $\chi 2$ versus period for a large number of realizations. The minimum $\chi 2$ corresponds to the planet period. *Bottom*: observed (dots) and fitted (solid line) *RV* versus time after folding of the time scale according to the fitted period.

5.2. Impact of the orbital radius

Similar conclusions are reached when considering a planet orbiting at 1 or 0.8 AU. Of course, the smaller the orbital radius, the larger the planet signal amplitude, and the easier it will be to detect the planet, for a given temporal sampling. We nevertheless note that the peak at the planet orbital period appears at a somewhat lower intensity in the case of $a = 1$ AU; this is because the planet orbit cannot be completely sampled because the planet period exactly matches the observability period of the star. This is illustrated in Fig. 18, where we show the periodograms obtained in the case of a temporal sampling of 4 days and a precision of 5 cm/s.

From the former two sections, we conclude that based on the present assumptions ($\Delta T_{\rm s} = 550$ K), a $1M_{\rm Earth}$ planet on a circular orbit in the HZ can be detected provided that the temporal sampling is good enough (more frequent than every 8 days), and long enough (covering at least 4 periods). The temporal sampling is therefore crucial to revealing the planet period and allowing a proper fit. This is very demanding in terms of telescope time but seems to be mandatory. In contrast, the precision (ranging between 1 cm/s and 10 cm/s) does not significantly impact the detectability of the planet.

5.3. Impact of the spot temperature

We then consider a spot temperature that is 1200 K below the Sun temperature, instead of 550 K. The cooler spots induce a higher (by factor 1.75) RV amplitude than those induced by the former spots. The effect is that for a given sampling, the peak produced by the planet in the periodograms is lower than that for $\Delta T_{\rm s} = 550$ K. Again the impact is stronger when considering the high activity period than the low activity period and the precision does not have a significant impact on the peak detectability. In Fig. 19, we compare the results for both cases, assuming that the star is observed every 4 days, and the precision is 5 cm/s.

The RV fitting now provides good results only when considering the low activity period and if the temporal sampling is the most frequent possible (every day over the observability period) or every 4 days.

6. Concluding remarks

We have computed the RV variations that would be caused by the set of spots observed on the Sun surface between 1993 and 2003. These variations are representative of the RV signatures that would be measured on a G2V star with a spot pattern and a rotation period identical to that of the Sun, seen edge-on. Our main results are the following:

– because of the large number of spots, RV variations are always present, with amplitudes of up to a few m/s if we

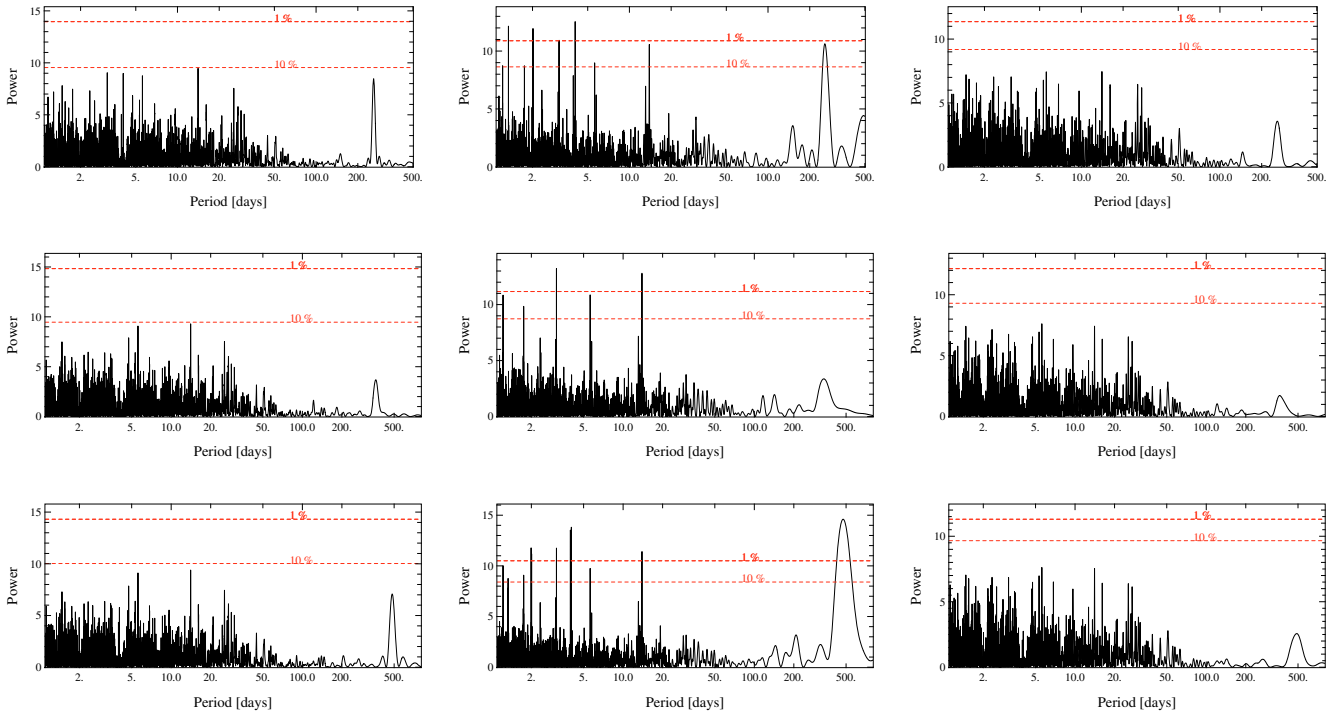

Fig. 18. Impact of the orbital radius. Periodograms corresponding to the RV of a spotted solar type star surrounded by a $1M_{\rm Earth}$ planet orbiting at resp. 0.8 (*top*), 1 (*middle*) and 1.2 (*bottom*) AU. The star is again assumed to be observable 8 months per year, and to be actually observed every 4 days, during the whole cycle (*Left*), the low (*Middle*) and high (*Right*) activity periods, with a precision of 5 cm/s.

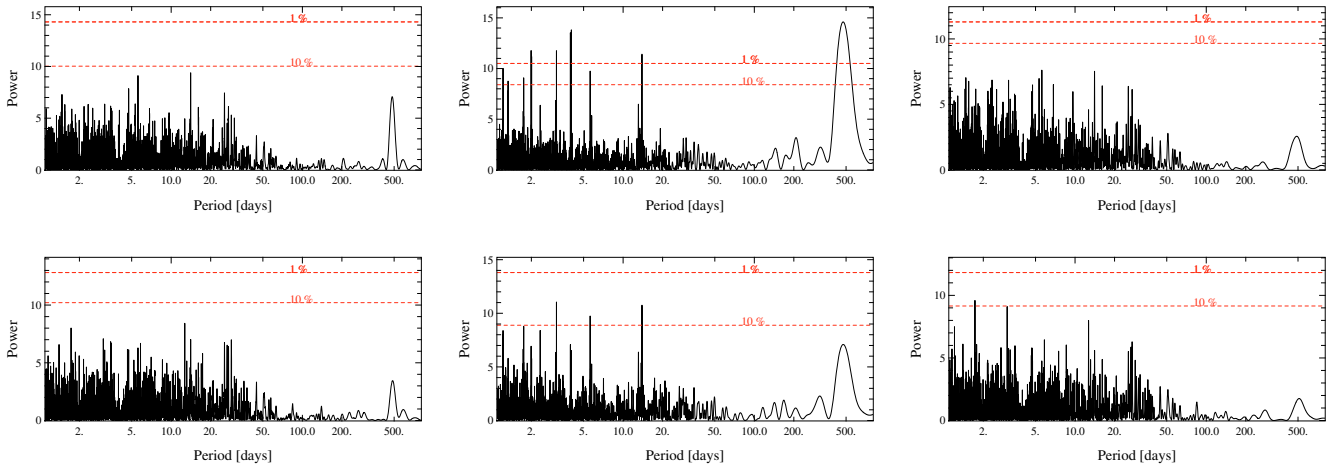

Fig. 19. Impact of the spots temperature. periodograms corresponding to the RV of a spotted solar type star surrounded by a 1 $M_{\rm Earth}$ planet orbiting at 1.2 AU. The spot temperature is either (*top*) or 1200 K (*bottom*) below the star effective temperature. The star is again assumed to be observable 8 months per year, and to be actually observed every 4 days, with a precision of 5 cm/s. From left to right, the whole cycle, the low activity period and the high activity period are considered.

assume the the spots are about 550 K cooler than the Sun photosphere;

- the RV amplitudes vary considerably, between 0.2 and 5 m/s, depending on the activity level. These amplitudes are larger those estimated for single spots, and are much larger than the ≃9 cm/s RV that would be induced by an Earth-mass planet orbiting at 1 AU from the star. During the low activity period, the RV curve is significantly more quiet and of much smaller amplitudes than during the high activity period;
- BVS variations do occur, but the amplitude of the (RV, BVS) slope is quite small, so that these variations would require data of very high precision (better than 5 cm/s) to be detectable during the low activity period;
- RV and BVS periodograms require large amount of data to yield significant results. They contain peaks at periods sometimes very different from the solar rotation period. This should be taken into account before attributing peaks at periods different from the star rotation period to planets rather than to spots;
- when assuming a spot that is cooler by 1200 K than the Sun, the amplitude of the RV or BVS curves increase by a factor 1.75;

– the simulated photometric variations are in close agreement with the spot signatures effectively observed on the Sun during the same period. The amplitude of the variations is relatively low, and would not, in particular, be detectable from the ground during the low activity period. During the low activity period, the comparison with the observed TSI also shows that even though the highest variations are caused by spots, the plages produce, a modulation of the TSI on timescales of the Sun rotation velocity. These plages could also affect the RV. On the other hand, during the high activity period, the TSI variations seem to be quite well matched to the spot-induced variations.

Simulations of a spotted solar-type star surrounded by a 1 $M_{\rm Earth}$ planet located in the HZ show that the planet period can be detected (with $\leq$1% false alarm probability) in the periodograms of the RV, provided that the star is observed sufficiently (more frequently than every 8 days), during a long period of time (at least 4 periods). The signal is far more clearly detected during the low activity period (much fewer spots are present), and RV fitting provides satisfactory recovery of the orbital parameters. During the high activity period, the planet signature can be identified, provided that excellent temporal coverage is obtained. The orbital parameters can be derived with greater difficulty. This means that detecting Earth-mass planets may in some cases (e.g., around stars with activity levels comparable to that of the active Sun, or stars with short observability periods) be hardly achievable and in any case require large allocations of telescope time. A data precision in a range 1−10 cm/s is not found to impact these results significantly, but on the other hand, help to identify the spot signatures.

The scenario developed in this paper is however very favorable, for several reasons:

– The planet is alone and on a circular orbit.
– The star is seen edge-on, hence the long-lived spots are hidden for half of the time. If the star is seen inclined, the spots may be observed all of the time and their signature, even though smaller in amplitude, is more comparable in shape to that also expected from planets (see Desort et al. 2007).
– The level of solar activity was rather low during the cycle considered.
– The spot temperature was assumed to be constant, only 550 K cooler than the Sun temperature, a value that happens to fit the Sun data quite well, but may be in the lowest range of possible values if we consider stars other than the Sun (Berdyugina 2005).
– No plages or convective flows were considered, altough we have shown that the impact of the plages on the RV of the Sun is not negligible, expecially during the low activity period. Hence, if solar-type stars with similar activity are also covered by plages similar to those of the Sun in addition to spots, their RV jitter will be higher, at least during the low activity period, than in the case described in this paper, which would have a strong and negative impact on Earth-mass planet detectability.

Acknowledgements. We acknowledge support from the French CNRS. We are grateful to Programme National de Planétologie (PNP, INSU), as well as to french Agence Nationale pour la Recherche, ANR. We thank Jérôme Bouvier for fruitful discussions, and Severine Pouchot for her participation. The spot data have been provided by the Debrecen Observatory. We acknowledge the Sacramento Peak Observatory of the U.S. Air Force Phillips Laboratory for providing the Ca index. The irradiance data set (version #25) have been provided by PMOD/WRC, Davos, Switzerland and we acknowledge unpublished data from the VIRGO experiment on the cooperative ESA/NASA mission SOHO. We also made use of the INSU/CNRS database BASS2000. Finally, we thank the referee for his/her comments.

References

Albregtsen, F., Joras, P. B., & Maltby, P. 1984, Sol. Phys., 90, 17
Berdyugina, S. V. 2005, Living Rev. Sol. Phys., 2, 8
Berdyugina, S. V., & Usoskin, I. G. 2003, AAP, 405, 1121
Chapman, G. A., Cookson, A. M., & Dobias, J. J. 1994, ApJ, 432, 403
Chapman, G. A., Cookson, A. M., Dobias, J. J., & Walton, S. R. 2001, ApJ, 555, 462
Deming, D., & Plymate, C. 1994, ApJ, 426, 382
Desort, M., Lagrange, A.-M., Galland, F., et al. 2007, A&A, 473, 983
D'Odorico, V., et al. 2007, Mem. Soc. Astron. Ital., 78, 712
Donati, J. F., & Collier-cameron, A. 1997, MNRAS, 291, 1
Ermolli, I., Criscuoli, S., Centrone, M., Giorgi, F., & Penza, V. 2007, A&A, 465, 305
Fligge, M., Solanki, S. K., Unruh, Y. C., Fröhlich, C., & Wehrli, Ch. 1998, A&A, 335, 709
Fligge, M., Solanki, S. K., & Unruh, Y. C. 2000, A&A, 353, 380
Foehlich, C. 2003, Geophys. Monograph Ser., 111, Am. Geophys. Union, Chap. 1
Fröhlich, C., & Lean, J. 1998, Geophys. Res. Lett., 25, 4377
Galland, F., Lagrange, A. M., Udry, S., et al. 2005a, A&A, 443, 337
Györi, L., Baranyi, T., Ludmany, A., & Mezo, G. 2003, Solar Variability as an Input to the Earth's Environement, Tatranská Lomnica, Slovakia, Proc. ISCS Symp., 707
Hall, J. C., Henry, G. W., Lockwood, G. W., et al. 2009, ApJ, 138, 312
Hatzes, A. P. 2002, Astron. Nachr., 323, 3/4, 392
Hempelmann, A. 2003, A&A, 399, 717
Huelamo, N., Figueira, P., Bonfils, X., et al. 2008, A&A, 489, L9
Huerta, M., Johns-Krull, C. M., Prato, L., et al. 2008, ApJ, 678, 472
Jimenez, A., Palle, P. L., Regulo, C., et al. 1986, AdSpR, 6, 89
Jones, B. W., Sleep, P. N., & Underwood, B. R. 2006, ApJ, 649, 1010
Kasting, J. F., Whitmire, D. P., & Reynolds, R. T. 1993, Icarus, 101, 108
Krivova, N. A., Solanki, S. K., Fligge, M., & Unruh, Y. C. 2003, A&A, 399, L1
Lanza, A. F., Rodon, M., & Pagano, I. 2007a, A&A, 425, 707
Lanza, A. F., Bonomo, A. S., & Rodon, M. 2007b, A&A, 464, 741
Livingston, W., Wallace, L., White, O. R., & Giampapa, M. S. 2007, ApJ, 657, 1137
Lockwood, G. W., Skiff, B. A., Henry, G. W., et al. 2007, ApJS, 171, 260
Mathew, S. K., Martinez Pillet, V., Solanki, S. K., & Krivova, N. A. 2007, A&A, 465, 291
McMillan, R. S., Moore, T. L., Perry, M. L., & Smith, P. H. 1993, ApJ, 403, 801
Mayor, M., Pepe, F., Queloz, D., et al. 2003, Messenger, 114, 20
Mayor, M., Bonfils, X., Forveille, T., et al. 2009, A&A, 507, 487
Meunier, N, Desort, M., & Lagrange, A. M. 2010, A&A, 512, A39
Mosser, B., Baudin, F., Lanza, A. F., et al. 2009, A&A, 506, 245
Noyes, R. W., Weiss, N. O., & Vaughan, A. H. 1984, ApJ, 287, 769
Saar, S. H., & Donnahue, R. A. 1997, ApJ, 485, 319
Skelly, M. B., Unruh, Y. C., Collier-Cameron, A., et al. 2009a, MNRAS, 385, 708
Skelly, M. B., Unruh, Y. C., Barnes, J. R., et al. 2009b, MNRAS, 399, 1829
Solanki, S. K. 2003, A&ARv, 11, 153
Solanki, S. K. 2007, ASPC, 368, 481
Wesolowski, M. J., Walton, S. R., & Chapman, G. A. 2008, Sol. Phys., 248, 141